https://doi.org/10.46813/2022-138-009

UDC 620.18, 356.7

STRUCTURE AND MECHANICAL PROPERTIES OF THE REFRACTORY MULTICOMPONENT ALLOYS OF THE Ta-Ti-V-Zr-Al SYSTEM

A. Levenets, M. Tikhonovsky, O. Velikodnyi, G. Rostova, I. Klimenko, G. Tolstolutska
National Science Center "Kharkov Institute of Physics and Technology", Kharkiv, Ukraine
E-mail: a.levenets@kipt.kharkov.ua

Refractory high-entropy alloys of the Ta-Ti-V-Zr-Al system, in which the V and Ta contents were varied, were investigated. Criteria, based on the thermodynamic parameters of the binary alloys, melting temperatures of the components, geometric and electronic characteristics of atoms, were used to calculate the possible phase-structural state of the alloys; results were compared with experimental data. Microstructural studies showed the presence of a typical dendritic structure in as-cast alloys with an average grain size of 40 μm, which depends on the concentration of the constituent elements. The microhardness of the alloys was theoretically calculated and experimentally investigated. It was found that the microhardness calculation, based on the data of the valence electrons concentration, bulk modulus and shear modulus, allows to estimate satisfactorily the value of microhardness.

INTRODUCTION

Refractory multicomponent concentrated alloys (RMCA) or refractory high-entropy alloys (RHEA) appeared after the expanding the concept of high-entropy (multicomponent) alloys, which differs significantly from the conventional alloys producing method, based on alloying a principal metal (i.e., Fe or Ni) with relatively small addition of other elements. These alloys have high strength characteristics and significant ductility in a wide temperature range, which makes them perspective for various applications [1]. Such alloys can be used in aviation and aerospace, as well as be the structural materials for next-gen (Gen IV) reactors [2].

RMCA laid in the center of multi of multidimensional phase diagram, i.e., multidimensional space "element – phase composition". More flexible change in the elemental composition gives the new possibilities to control the properties of such materials. Combination of elements with high melting point leads to the formation of phases in the structure that are able to maintain their strength characteristics at high temperature [3]. In particular, this applies to light alloys based on Ti, Zr, V and Ta. The mechanical properties of such alloys can be compared with Ni-superalloys without heat treatment, for example, with Haynes 230 [4]. Yield strength of some RHEA is 500…700 MPa at 1200 °C, which exceeds the value of conventional Ni-based refractory alloys [5, 6]. Refractory HEA with the best high-temperature characteristics are usually single-phased with disordered solid solution structure [7]. Multiphase RHEA are stronger than single-phased at temperatures below 800…1000 °C, although they quickly lose strength with increasing temperature due to dissolution of the second phases [8]. However, relatively few alloys did have an experimentally confirmed single-phase bcc structure. The structure of RHEA systems, including Ti, Nb, Ta, Mo, and Zr, is a double bcc phase with dendritic morphology and heterogeneous composition [9]. One of the most investigated refractory alloys TiZrNbHfTa has high mechanical properties in a wide temperature range, as well as significant plasticity, allowed to withstand severe deformations [10, 11]. Yield strength of the alloys of Mo-Nb-Ta-Ti-Zr system is lower than for the double phased Ni-refractory alloys (i.e., Inconel 718), so it began to be doped with Al [12]. Such alloys are stronger at compression at high temperatures and have lower density. However, a large amount of aluminum can lead to embrittlement of grain boundaries and formation of intragranular precipitations enriched with Al and Zr [13]. The aim of this work was to study the structure and properties of refractory Ta-Ti-V-Zr-Al alloys, which are of great interest both to compare the predicted and experimentally determined structure properties and study further the complex of their properties.

MATERIALS AND METHODS

The HEA ingots of $Ta_{29-x}Ti_{40}V_xZr_{26}Al_5$ system with x = 0, 5, 10, 15, 20, 29 were obtained by arc melting with a non-consumable tungsten electrode on a massive copper hearth in an argon atmosphere. The melting was carried out in a multi-position mold, allowing to melt several ingots in one load. The specimens for microstructure were produced from the received ingots by spark cutting.

The microstructure of as-cast samples was studied using a metallographic inversion microscope Olympus GX51 and scanning electron microscope JSM 7001F equipped with a system for energy-dispersive X-ray spectroscopy (EDS) INCA ENERGY 350. The integral chemical composition was measured by X-ray fluorescence spectrometer (XRF) "SPRUT-V". Specimens for LM and SEM observations were prepared by a standard metallographic process (ground up to #1200 with SiC papers and polished with diamond paste). To reveal the microstructure, a freshly prepared etchant was used, consisting of 1 part of HNO_3, 1 part of HF, 1 part of H_2O and a few drops of H_2SO_4.

X-ray diffraction (XRD) patterns of the as-cast specimens were recorded using "DRON-4-07" diffractometer equipped with a Bragg-Brentano geometry, a Cu-Kα radiation source, a Ni absorbing filter and a scintillation detector. Standard processing (background removing, $K\alpha_2$ reduction, diffraction peaks fitting by pseudo-Voigt function) was applied for all diffraction patterns to obtain the peak characteristics (diffraction angle 2θ, integral intensity *I*, integral breadth *B*, interplanar spacing *d*) needed for further calculations. Qualitative phase analysis was performed using Crystallography Database ICDD PDF-2.

A microindentation method was used to study the mechanical properties as it provides a large number of measurements on a small surface of the same sample and permits data based on good statistics.

RESULTS

PREDICTED PHASE CONSTITUTION AND STRUCTURE

Theoretical prediction of phase constitution and crystal phase structure, which formed in the alloy, is extremely important because there are a large number of possible alloy composition with the presence of 4–5 components. Phase state of the alloy is usually determined by the phase diagrams. Traditionally, these diagrams are obtained from experiments. Such approach is possible for binary and simple triple systems but is extremely difficult for complex multicomponent systems. Calculating methods for constructing the phase diagram have been recently developed (CALPHAD). However, they do not always give the good results due to the flaw and inaccuracy of the thermodynamic parameters. In this regard, the number of semi-empirical criteria have been proposed, which allowed to predict the main parameters for the multicomponent alloys with a certain degree of confidence. These criteria are based on the Hume-Rothery rules for binary alloys, adapted for the multicomponent system. Table 1 shows the discussed parameters for further investigations.

According to the literature data, there are several criteria for prediction the phase state. These criteria were verified experimentally, and their value vary from source to source. The same alloy can relate as to simple solid solution, as to solution with intermetallic phase as per the criteria. The criteria will be conventionally named as A, B, C, and D. These criteria are shown in Table 2.

The criterion A considers a correlation between the ΔS_{mix}, ΔH_{mix}, and δ. It was established after the comparing the calculated and experimental (on the structure state formed during the crystallization) values of mentioned parameters that a simple disordered solid solution preferentially forms at the high mixing entropy, low mixing enthalpy and low atomic size mismatch. An alloy with the low negative mixing enthalpy is more prone to form the intermetallic compounds. However, the limit values of the parameters are noticeably different according to the different literature sources. There are at least three various boundary condition, marked as A1, A2, and A3.

Table 1

Main parameters to assess the structural-phase composition of high-entropy alloys

Property	Formula	
mixing entropy	$\Delta S_{mix} = -R\sum_{i=1}^{n} c_i ln c_i$ $R = 8.314\ \mathrm{J\cdot mol^{-1}}K^{-1}$	c_i – concentration of the i-th element
mixing enthalpy	$\Delta H_{mix} = \sum_{i=1,i\neq j}^{n} \Omega_{ij} c_i c_j$ $\Omega_{ij} = 4\Delta_{mix}^{AB}$	Δ_{mix}^{AB} – enthalpy of equiatomic binary AB alloy $c_{i(j)}$ – concentration of the i(j)-th element
atomic size mismatch	$\delta = 100 \times \sqrt{\sum_{i=1}^{n} c_i (1 - {r_i}/{\bar{r}})^2}$ $\bar{r} = \sum_{i=1}^{n} c_i r_i$	r_i – atomic radius of the i-th element
valence electron concentration	$VEC = \sum_{i=1}^{n} c_i (VEC)_i$	$(VEC)_i$ – valence electron concentration of i-th element
electronegativity	$\Delta\chi = \sqrt{\sum_{i=1}^{n} c_i (\chi_i - \bar{\chi})^2}$ $\bar{\chi} = \sum_{i=1}^{n} c_i \chi_i$	χ_i – Pauling electronegativity of i-th element
dimensionless parameter Ω	$\Omega = \frac{T_m \Delta S_{mix}}{\lvert\Delta H_{mix}\rvert}$ $T_m = \sum_{i=1}^{n} c_i (T_m)_i$	T_m – average melting temperature of the elements

Table 2

Criteria for determining the phase composition and crystal lattice of HEA

Criterion A: correlation between ΔS_{mix}, ΔH_{mix}, and δ			
A1	$-15 \le \Delta H_{mix} \le 5$ kJ/mol $0 < \delta < 5$	simple disordered solid solution	[14]
	$-20 \le \Delta H_{mix} \le 0$ kJ/mol $5 < \delta < 6.6$	disordered solid solutions	[15]
A2	$-22 \le \Delta H_{mix} \le 7$ kJ/mol $0 \le \delta \le 8.5$ $11 \le \Delta S_{mix} \le 19.5$ J/kmol	solid solution	[16]
A3	$-10 \le \Delta H_{mix} \le 5$ kJ/mol $\delta < 4$ $\Delta S_{mix} > 13.38$ J/kmol	simple solid solution	[17]
	$50 \le \Delta H_{mix} \le 0$ kJ/mol $4 \le \delta \le 20$ $4 \le \Delta S_{mix} \le 18$ J/kmol	amorphous phase	[18]
Criterion B: correlation between Ω and δ			
B	$\Omega > 1.1$ $\delta < 6.6$	solid solution	[19]
Criterion C: correlation between VEC and δ			
C1	$\delta < 5$	FCC lattice	[20]
	$\delta > 5.4$	BCC lattice	
C2	VEC ≥ 8	FCC lattice	[14]
	VEC < 6.87	BCC lattice	
C3	4,33 < VEC < 7.55	BCC lattice	[21]
	7,80 < VEC < 9.50	FCC lattice	
C4	4,2 $\le$ VEC $\le$ 7.2	BCC lattice	[22]
	VEC $\ge$ 7.5	FCC lattice	
Criterion D: correlation between $\Delta\chi$ and δ			
D	$0.03 < \Delta\chi < 0.06$ $1 < \delta < 6$	no intermetallic compounds	[23]
	$\Delta\chi \approx 0.09…0.14$ $\delta \approx 6$	appearance of compounds (intermetallic, σ-phase)	

A1: According to [14], a simple disordered solid solution forms at $-15 \le \Delta H_{mix} \le 5$ kJ/mol and $0 < \delta < 5$. Ordered and disordered solid solutions form in a transition zone, which is in range of $-20 \le \Delta H_{mix} \le 0$ kJ/mol and $5 < \delta < 6.6$ [15].

A2: According to [16], a solid solution forms at $-22 \le \Delta H_{mix} \le 7$ kJ/mol, $0 \le \delta \le 8.5$ and $11 \le \Delta S_{mix} \le 19.5$ J/kmol.

A3: According to [17], a simple solid solution forms at $\Delta S_{mix} > 13.38$ J/kmol, $-10 \le \Delta H_{mix} \le 5$ kJ/mol and $\delta < 4$.

According to the experimental data, an amorphous phase forms in wide range of these parameters: $-50 \le \Delta H_{mix} \le 0$ kJ/mol; $4 \le \delta \le 20$; $4 \le \Delta S_{mix} \le 18$ J/kmol [18].

The criterion B depends on the Ω and δ. According to [19], the high $\Omega > 1.1$ and low $\delta < 6.6$ values agree with the solid solution formation in multicomponent alloys.

The criterion C uses the relationship between VEC та δ for predicting the preferred type of crystal lattice formed in the alloy. Specific values according to the authors will be marked as C1, C2, C3, and C4.

C1: According to [20], FCC lattice forms at $\delta < 5$ and BCC lattice forms at $\delta > 5.4$.

C2: According to [14], FCC lattice tends to form at high VEC (VEC $\ge$ 8) and BCC lattice tends to form at low VEC (VEC < 6.87).

C3: According to [21], valence electron concentration range has the following limits: from 4.33 to 7.55 – BCC, from 7.80 to 9.50 – FCC.

C4: According to [22], the VEC values, indicating on the BCC structure, are lower than in other sources, viz 4.2 $\le$ VEC $\le$ 7.2. FCC structure forms at VEC $\ge$ 7.5.

The criterion D depends on the $\Delta\chi$ and δ. According to [23], no intermetallic compounds form at $1 < \delta < 6$ and $0.03 < \Delta\chi < 0.06$. Appearance of compounds in solid solution (SS+Im, SS+σ) is likely belongs to the following range: $\delta \approx 6$, $\Delta\chi \approx 0.09…0.14$.

The predicted structural states of the studied alloys, which follow from the calculated parameters (Table 3), are shown in Table 4.

Table 3

Parameters for $Ta_{29-x}Ti_{40}V_xZr_{26}Al_5$ alloys

Alloy (x value)/ parameter	VEC	δ	$\Delta\chi$	ΔS_{mix}, J/kmol	ΔH_{mix}, kJ/mol	Ω
x = 0	4.24	4.68	0.09	10.19	-6.50	3.6
x = 5	4.24	5.28	0.10	11.30	-7.08	3.6
x = 10	4.24	5.80	0.10	11.74	-7.65	3.4
x = 15	4.24	6.26	0.11	11.86	-8.19	3.1
x = 20	4.24	6.67	0.11	11.68	-8.72	2.8
x = 29	4.24	7.32	0.12	10.19	-9.61	2.1

It can be seen, that according to the A2, C2, C4 criteria, each alloy has to form solid solution with BCC structure. According to the A1, A3, and C3 criteria, all the alloys are located in the transition zone, but by the B and C1 criteria only some alloys are located in that zone, although the values of calculated parameters are close to the area of simple solid solution with BCC lattice existence. In accordance with the criterion D, all the alloys are solid solutions with a high probability of intermetallic or sigma-phase presence.

Table 4

The predicted structure[1] for $Ta_{29-x}Ti_{40}V_xZr_{26}Al_5$ alloys

Alloy (x value)/ criterion	A1	A2	A3	B	C1	C2	C3	C4	D
x = 0	SDSS	DSS?	TZ	DSS	FCC	BCC	BCC (TZ?)	BCC	DSS (Im (σ)?)
x = 5	TZ	DSS	TZ	DSS	BCC (TZ?)	BCC	BCC (TZ?)	BCC	DSS (Im (σ)?)
x = 10	TZ	DSS	TZ	DSS	BCC	BCC	BCC (TZ?)	BCC	DSS (Im (σ)?)
x = 15	TZ	DSS	TZ	DSS	BCC	BCC	BCC (TZ?)	BCC	Im (σ)
x = 20	TZ	DSS	TZ	DSS (TZ?)	BCC	BCC	BCC (TZ?)	BCC	Im (σ)
x = 29	TZ?	DSS	TZ	DSS (TZ?)	BCC	BCC	BCC (TZ?)	BCC	Im (σ)

STRUCTURE INVESTIGATIONS

X-ray studies. Calculated lattice parameter a_c was determined be the average atomic radius r_{av}. For bcc lattice

$$a_c = \frac{4r_{av}}{\sqrt{3}}, \quad r_{av} = \sum_i r_i \cdot c_i\,, \qquad (1)$$

where r_i is the atomic radius of i-th element and c_i is the concentration of i-th element (r_{Al} = 1.43 Å; r_{Ta} = 1.46 Å; r_{Ti} = 1.47 Å; r_V = 1.34 Å; r_{Zr} = 1.60 Å).

Calculations of X-ray density ρ_X was performed by the equation

$$\rho_X = \frac{M}{N_A \cdot V}\,, \qquad (2)$$

where M is the molar mass; N_A is the Avogadro number and V is the unit cell volume. Fig. 4 shows a diffraction pattern of the alloys and calculated parameters and phase structure are presented in Table 5.

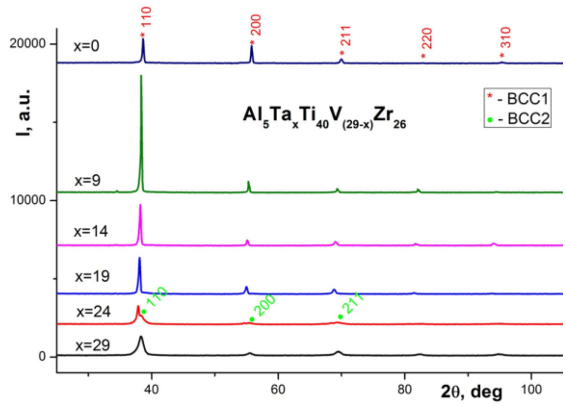

Fig 1. Diffractograms of the $Ta_{29-x}Ti_{40}V_xZr_{26}Al_5$ alloys

Table 5

Lattice parameters and substructural parameters of $Ta_{29-x}Ti_{40}V_xZr_{26}Al_5$ alloys

Alloy (x value)	Phase structure	Lattice parameter *a*, Å	Calculated lattice parameter a_c, Å	a/a_c	Unit cell volume V, $Å^3$	X-ray density ρ_X, g/cm^3
0	BCC	3.309	3.462	0.956	36.23	8.864
5	BCC 1	3.362	3.448	0.975	38.00	7.883
	BCC 2	3.313		0.961	36.36	8.238
10	BCC 1	3.341	3.434	0.973	37.29	7.454
	BCC 2	3.257		0.948	34.55	8.045
15	BCC	3.332	3.420	0.974	36.99	6.931
20	BCC	3.319	3.406	0.974	36.56	6.422
29	BCC 1	3.296	3.381	0.975	35.81	5.472
	BCC 2	3.384		1.001	38.75	5.056

[1] TZ – transition zone, DSS – disordered solid solution, SDSS – simple disordered solid solution, BCC – body-centered cubic lattice, FCC – face-centered cubic lattice, Im (σ) –intermetallic phase (or σ-phase)

In the absence of vanadium (x = 0), sample has single-phase bcc structure with lattice parameter a = 3.309 Å. The diffraction pattern of this alloy shows the diffraction line broadening of bcc phase, so substructural characteristics were estimated (values of coherent-scattering domain (CSD) sizes D and microstrains ε). CSD size for bcc phase is D = 7.1 nm at a low level of microdeformations $\varepsilon = 5 \cdot 10^{-4}$, i.e., the greatest contribution to the line broadening gave CSD size. With maximum vanadium concentration (x = 29) there are two identified bcc phases. The lattice parameter of bcc1 phase is a = 3.296 Å, and lattice parameter of bcc2 phase is a = 3.384 Å, moreover the content of this phase in the sample is very small, according to the diffraction lines intensity. Also, the diffractogram contains a low-intensity line at diffraction angle 2θ = 59.26°, which does not belong to the mentioned above phases. That is, the sample contains a small amount of the third phase, which could not be identified. Samples with x = 5 and 10 are two-phased, and in the last sample the content of bcc2 phase is very small, as evidenced by the relative intensity of the lines of this phase.

Microstructure. Metallographic investigations have shown that all the alloys have a similar microstructure, characterized by the presence of grains, within with a dendritic liquation is observed. An example of alloy microstructure is shown on Fig. 2.

The average grain size increases with increasing of vanadium concentration in the alloy, i.e., with the x growth, and is 29, 432, 46, and 50 µm for x = 5, 10, 15, and 20, respectively. The average grain size for the alloys with x = 0 and 29 does not fall under this pattern, and is 31.1 and 40 µm, accordingly.

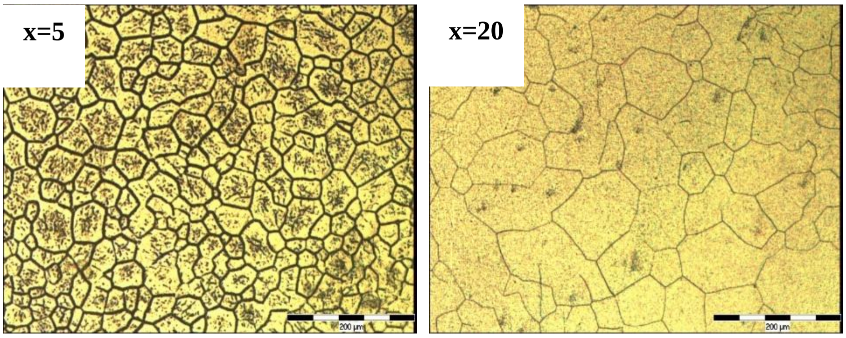

Fig. 2. Optical micrographs of $Ta_{29-x}Ti_{40}V_xZr_{26}Al_5$ alloys with x = 5 and 20

The actual composition of the alloys, determined by the XRF method, corresponds quite well to the nominal composition. However, Al concentration turned to be lower than the nominal by 0.25…0.5 at.%, and Ti concentration is higher than the nominal one by 1…2 at.%. Wherein, EDS analysis has shown that the content of individual elements in dendrites and interdendritic areas differs noticeably. Characteristic maps of elemental distribution in the alloys with x = 5 and 20 are shown on Fig. 3.

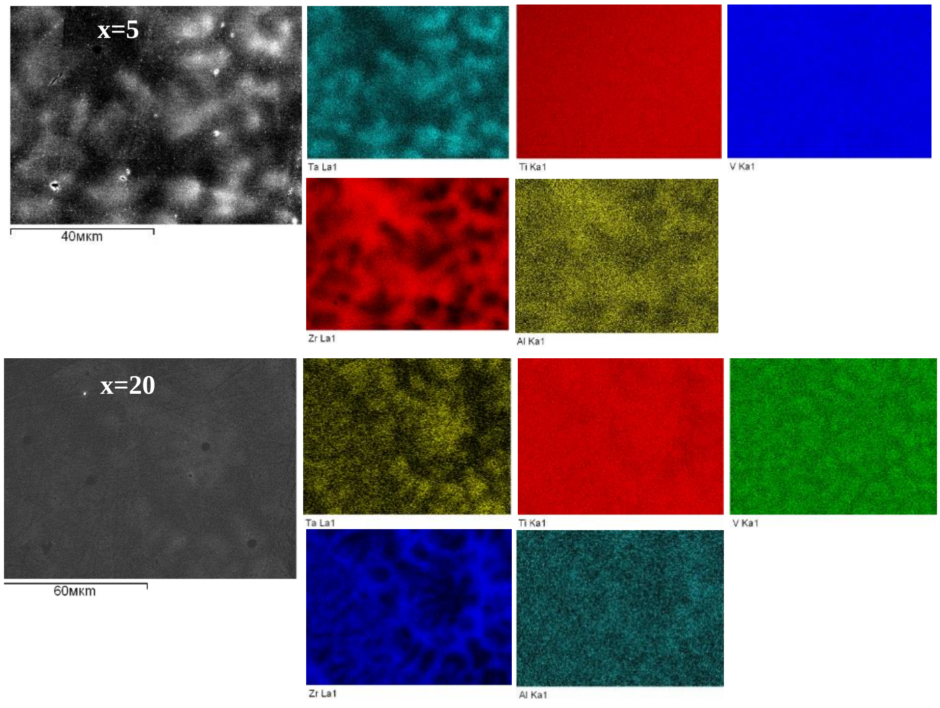

Fig. 3. The EDS elemental maps of the $Ta_{29-x}Ti_{40}V_xZr_{26}Al_5$ alloys with x = 5 and 20

It can be seen from the presented images, that Ti and V are distributed uniformly through the microstructural components, whereas Ta significantly enriches dendrites and Zr is located in the interdendritic areas. Moreover, Al is located in the interdendritic space as well. These data are in agreement with the results of the quantitative elemental analysis for dendrites and interdendrites, performed by EDS, which are presented in the Table 6.

The increased Ta concentration in dendrites is only natural, since it is the most refractory element in the alloy system. And, the solidification starts from the nucleation and growth of the dendrites, which composition corresponds to the highest crystallization temperature. Wherein, the fewer refractory elements are pushed into a liquid, which solidifies in the interdendritic areas last. However, the level of liquid enrichment with one or another element is determined not only by its melting temperature, but by the corresponding distribution coefficient.

Table 6

Concentration of the metallic elements in the dendrites (D) and interdendritic regions (ID)

Regions	Ta	Ti	V	Zr	Al
x = 0					
Nominal composition	29	40	–	26	5
D	39.23	37.01	–	20.25	3.51
ID	19.51	40.46	–	33.34	6.70
x = 5					
Nominal composition	24	40	5	26	5
D	28.39	39.97	5.36	22.78	3.50
ID	18.71	42.19	5.51	28.19	5.40
x = 10					
Nominal composition	19	40	10	26	5
D	22.09	41.83	11.51	20.67	3.89
ID	14.54	41.45	10.87	28.29	4.85
x = 15					
Nominal composition	14	40	15	26	5
D	11.19	42.42	15.38	26.40	4.61
ID	10.07	40.97	15.51	28.40	4.75
x = 20					
Nominal composition	9	40	20	26	5
D	10.76	43.30	19.64	22.41	3.88
ID	6.84	41.30	19.51	27.51	4.84
x = 29					
Nominal composition	–	40	29	26	5
D	–	40.34	25.72	29.05	4.89
ID	–	43.97	30.15	20.06	5.82

Mechanical properties

Theoretical prediction of microhardness, according to [24], can be performed by its connection with the bulk and shear modulus by the equation (3)

$$H_v = 2(k^2G)^{0.585} - 3, k = {}^{G}/_{B}, \quad (3)$$

$$G = \sum_{i=1}^{n} c_i G_i s, \quad (4)$$

$$B = \sum_{i=1}^{n} c_i B_i \,. \quad (5)$$

Bulk modulus (5) determines only the isotropic resistance to deformation, while the shear modulus (4) is responsible for the anisotropic resistance. Coefficient k (3) impacts on the Vickers microhardness, i.e., if the bulk modulus increases, the microhardness will decrease with the constant shear modulus, and vice versa. Material becomes more ductile if the ratio k decreases with bulk modulus increasing [25].

Furthermore, it was proposed for high-entropy alloys to use the relationship between microhardness and valence electron concentration VEC [26] as followed

$$H_\mu \sim (VEC)^2 R_n^{-1} \quad . \quad (6)$$

The load on the indenter at experimental determinations of Vicker microhardness was 1 N and for each sample was performed for 10 indentations along the surface section at regular intervals. The microhardness of the samples is approximately at the same level, while two-phase alloys with x = 5 and 10 show higher values than single-phase alloys. The highest value of microhardness of 3.8 GPa is observed in the alloy with x = 0 with the highest tantalum content in the alloy. Hardness values decrease with increasing V content, which is associated with an increase in grain size. However, microhardness of $Ta_{29-x}Ti_{40}V_xZr_{26}Al_5$ alloys is higher than that of many refractory alloys reported in the literature.

Table 7

Experimental and calculated microhardness of $Ta_{29-x}Ti_{40}V_xZr_{26}Al_5$ alloys

Microhardness, GPa	x=0	x=5	x=10	x=15	x=20	x=29
Experimental	4.71±0.1	3.88±0.1	3.72±0.1	3.36±0.04	3.53±0.1	3.62±0.1
Theoretical (1)	3.57	3.26	3.15	3.04	2.93	2.90
Theoretical (2)	2.92	2.78	2.65	2.51	2.38	2.13

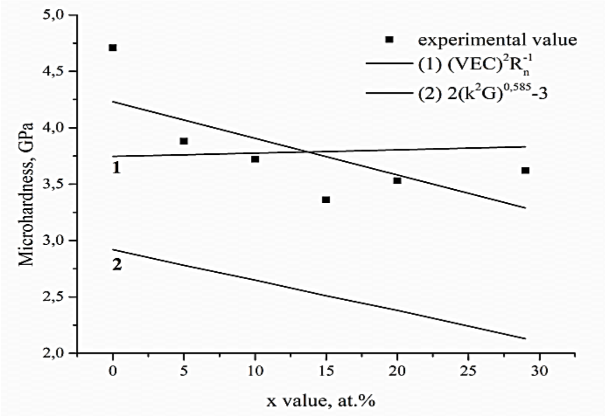

Fig. 4. Experimental and calculated microhardness of $Ta_{29-x}Ti_{40}V_xZr_{26}Al_5$ alloys

Theoretical and experimental values of microhardness are given in Table 7. Experimental values are much higher than calculated, but there is an approximately equal ratio between the values of microhardness. This may be due to the fact that the coefficients in (8) were taken on the basis of assumptions for HEA as a whole and may be different for a particular system of multicomponent alloys. The calculation of microhardness based on the concentration of valence electrons (Fig. 4, curve 1) gives closer to the real values, but the course of the dependence Hμ (x) differs significantly from that obtained experimentally. On the other hand, the calculation based on modules (see Fig. 4, curve 2) shows a similar trend to the experimental one. Further research in obtaining the correct coefficients for such RHEA system is needed.

CONCLUSIONS

1. Using the thermodynamic parameters for binary alloys, melting temperatures, geometric and electronic characteristics of components, calculations of the predicted phase composition of $Ta_{29-x}Ti_{40}V_xZr_{26}Al_5$ alloys were performed. The predicted regions of concentrations within which single-phase states with bcc lattices are realized, as well as regions with heterophase structure, and phase composition of these regions are established.

2. Experimental and predicted composition of $Ta_{29-x}Ti_{40}V_xZr_{26}Al_5$ alloys correlate well with each other. XRD analysis shows that alloys with x = 5, 10 and 29 have two bcc phases, and alloys with x = 0, 15 and 20 have single-phase structure with bcc lattice. The homogeneity of the samples was shown by EDS and XRF methods.

3. The methods of metallography and electron microscopy revealed a typical structure for such a system of alloys with an average grain size of 40 μm.

4. Microhardness of $Ta_{29-x}Ti_{40}V_xZr_{26}Al_5$ alloys is at the level of 3.4…3.9 GPa, which is higher than that of many refractory alloys reported in the literature.

5. Calculated microhardness based both on the valence electron concentration and the bulk and shear modules dependence allows to establish the order of real microhardness values, moreover the VEC dependence gives closer to the experimental values.

ACKNOWLEDGEMENTS

This work was supported by the National Research Foundation of Ukraine in frame of the project №2020.02/0327 "Fundamental aspects of the new materials creation with unique physical, mechanical and radiation properties based on the concentrated multicomponent alloys".

REFERENCES

1. O.N. Senkov, S. Gorsse, D.B. Miracle. High temperature strength of refractory complex concentrated alloys // *Acta Materialia*. 2019, v. 175, p. 394-405; http://dx.doi.org/10.1016/j.actamat.2019.06.032

2. A. Motallebzadeh, N.S. Peighambardoust, S. Sheikh, H. Murakami, S. Guo, D. Canadinc. Microstructural, mechanical and electrochemical characterization of TiZrTaHfNb and Ti1.5ZrTa0.5Hf0.5Nb0.5 refractory high-entropy alloys for biomedical applications // *Intermetallics*. 2019, v. 113, p. 106572; http://dx.doi.org/10.1016/j.intermet.2019.106572

3. D.B. Miracle, O.N. Senkov. A critical review of high entropy alloys and related concepts // *Acta Materialia*. 2017, v. 122, p. 448-511; https://doi.org/10.1016/j.actamat.2016.08.081

4. O.N. Senkov, G.B. Wilks, J.M. Scott, D.B. Miracle. Mechanical properties of Nb25Mo25Ta25W25 and V20Nb20Mo20Ta20W20 refractory high entropy alloys // *Intermetallics*. 2011, v. 19, p. 698-706; https://doi.org/10.1016/j.intermet.2011.01.004

5. Y. Zou, J.M. Wheeler, H. Ma, P. Okle, R. Spolenak. Nanocrystalline High-Entropy Alloys: A New Paradigm in High-Temperature Strength and Stability // *Nano Letters*. 2017, v. 17(3), p. 1569-1574; https://doi.org/10.1021/acs.nanolett.6b04716

6. Y.D. Wu, Y.H. Cai, T. Wang, J.J. Si, J. Zhu, Y.D. Wang, X.D. Hui. A refractory $Hf_{25}Nb_{25}Ti_{25}Zr_{25}$ high-entropy alloy with excellent structural stability and tensile properties // *Materials Letters*. 2014, v. 130, p. 277-280; https://doi.org/10.1016/j.matlet.2014.05.134

7. D. Miracle, M.-H. Tsai, O. Senkov, V. Soni, R. Banerjee. Refractory high entropy superalloys (RSAs) // *Scripta Materialia*. 2020, v. 187, p. 445-452; https://doi.org/10.1016/j.scriptamat.2020.06.048

8. O.N. Senkov, S.V. Senkova, C. Woodward, D.B. Miracle. Low-density, refractory multi-principal element alloys of the Cr–Nb–Ti–V–Zr system: Microstructure and phase analysis // *Acta Materialia*. 2013, v. 61(5), p. 1545-1557; https://doi.org/10.1016/j.actamat.2012.11.032

9. J. Normand, R. Moriche, C. García-Garrido, R.E. Sepúlveda Ferrer, E. Chicardi. Development of a TiNbTaMoZr-Based High Entropy Alloy with Low Young´s Modulus by Mechanical Alloying Route // *Metals*. 2020, v. 10(11), p. 1463; https://doi.org/10.3390/met10111463

10. J.P. Couzinie´, G. Dirras, L. Perrie`re, T. Chauveau, E. Leroy, Y. Champion, I. Guillot. Microstructure of a near-equimolar refractory high-entropy alloy // *Materials Letters*. 2014, v. 126, p. 285-287; http://dx.doi.org/10.1016/j.matlet.2014.04.062

11. B. Schuh, B. Volker, J. Todt, N. Schell, L. Perrie`re, J. Li, J.P. Couzinie´, A. Hohenwarter. Thermodynamic instability of a nanocrystalline, single-phase TiZrNbHfTa alloy and its impact on the mechanical properties // *Acta Materialia*. 2018, v. 142, p. 201-242; https://doi.org/10.1016/j.actamat.2017.09.035

12. T.E. Whitfield, E.J. Pickering, L.R. Owen, C.N. Jones, H.J. Stone, N.G. Jones. The effect of Al on the formation and stability of a bcc - B2 microstructure in a refractory metal high entropy superalloy system // *Materialia*. 2020, v. 13, p. 100858; https://doi.org/10.1016/j.mtla.2020.100858

13. K. Jensen, Characterization of a High Strength, Refractory High Entropy Alloy, AlMo0.5NbTa0.5TiZr. PhD Dissertation, The Ohio State University, Columbus, OH, USA, 2017. AAT 10659912

14. J. Málek, J. Zýka, F. Lukáˇc, M. Vilémová, T. Vlasák, J. Čížek, O. Melikhova, A. Macháˇcková, H.-S. Kim. The Effect of Processing Route on Properties of HfNbTaTiZr High Entropy Alloy // *Materials*. 2019, v. 12(23), p. 4022; https://doi.org/10.3390/ma12234022

15. J.-C. Zhu, M. Liao, Y. Liu, P. Cui, N. Qu, F. Zhou, D. Yang, T. Han, Z. Lai. Modeling of alloying effect on elastic properties in BCC Nb-Ti-V-Zr solid solution: From unary to quaternary // *Computational Materials Science*. 2020, v. 172, p. 109289; http://dx.doi.org/10.1016/j.commatsci.2019.109289

16. J. Montero, G. Ek, L. Laversenne, V. Nassif, G. Zepon, M. Sahlberg, C. Zlotea. Hydrogen storage properties of the refractory Ti-V-Zr-Nb-Ta multi-principal element alloy // *Journal of Alloys and Compounds*. 2020, v. 835, p. 155376; https://doi.org/10.1016/j.jallcom.2020.155376

17. D.N. Klimenko, N. Yurchenko, N.D. Stepanov, S. Zherebtsov. Prediction of strength characteristics of high-entropy alloys Al-Cr-Nb-Ti-V-Zr systems // *Materials Today: Proceedings*. 2021, v. 38, p. 1535-1540; https://doi.org/10.1016/j.matpr.2020.08.145

18. N.Yu. Yurchenko, N.D. Stepanov, A.O. Gridneva, M.V. Mishunin, G.A. Salishchev, S.V. Zherebtsov. Effect of Cr and Zr on phase stability of refractory Al-Cr-Nb-Ti-V-Zr high-entropy alloys // *Journal of Alloys and Compounds*. 2018, v. 757, p. 403-414; https://doi.org/10.1016/j.jallcom.2018.05.099

19. J. Zheng, X. Hou, X. Wang, Y. Meng, X. Zheng, L. Zheng. Isothermal oxidation mechanism of Nb–Ti–V–Al–Zr alloy at 700–1200 °C: Diffusion and interface reaction // *Corrosion Science*. 2015, v. 96, p. 186-195; https://doi.org/10.1016/j.corsci.2015.04.002

20. D.J.M. King, S.T.Y. Cheung, S.A. Humphry-Baker, C. Parkin, A. Couet, M.B. Cortie, G.R. Lumpkin, S.C. Middleburg, A.J. Knowles. High temperature, low neutron cross-section high-entropy alloys in the Nb-Ti-V-Zr system // *Acta Materialia*. 2019, v. 166, p. 435-446; https://doi.org/10.1016/j.actamat.2019.01.006

21. U. Jain, A. Mukherjee, G.K. Dey. Thermodynamic properties of Ti in V-Ti-Ta alloys: Effect of Ta addition // *Journal of Alloys and Compounds*. 2016, v. 686, p. 946-950; https://doi.org/10.1016/j.jallcom.2016.06.200

22. V.F. Gorban, N.A. Krapivka, S.A. Firstov. High-entropy alloys: Interrelations between electron concentration, phase composition, lattice parameter, and properties // *Physics of Metals and Metallography*. 2017, v. 118, p. 970-981; https://doi.org/10.1134/S0031918X17080051

23. M.G. Poletti, L. Battezzati. Electronic and thermodynamic criteria for the occurrence of high entropy alloys in metallic systems // *Acta Materialia*. 2014, v. 75, p. 297-3064; https://doi.org/10.1016/j.actamat.2014.04.033

24. X.-Q. Chen, H. Niu, D. Li, Y. Li. Modeling hardness of polycrystalline materials and bulk metallic glasses // *Intermetallics*. 2011, v. 19(9), p. 1275-1281; https://doi.org/10.1016/j.intermet.2011.03.026

25. U. Bhandari, C. Zhang, C. Zeng, S. Guo, A. Adhikari, S. Yang. Deep Learning-Based Hardness Prediction of Novel Refractory High-Entropy Alloys with Experimental Validation // *Crystals*. 2021, v. 11(1), p. 46; https://doi.org/10.3390/cryst11010046

26. J. Wang, S. Bai, Y. Tang, S. Li, X. Liu, J. Jia, Y. Ye, L. Zhu. Effect of the valence electron concentration on the yield strength of Ti-Zr-Nb-V high-entropy alloys // *Journal of Alloys and Compounds*. 2021, v. 868, p. 159190; https://doi.org/10.1016/j.jallcom.2021.159190

Article received 04.02.2022

СТРУКТУРА ТА МЕХАІЧНІ ВЛАСТИВОСТІ ТУГОПЛАВКИХ БАГАТОКОМПОНЕНТНИХ СПЛАВІВ СИСТЕМИ Ta-Ti-V-Zr-Al

А. Левенець, М. Тихоновський, О. Великодний, Г. Ростова, І. Клименко, Г. Толстолуцька

Було досліджено тугоплавкі високоентропійні сплави системи Ta-Ti-V-Zr-Al, в якій варіювався вміст V та Ta. Було запропоновано критерії на основі термодинамічних параметрів для бінарних сплавів, температур плавлення компонентів, геометричних та електронних характеристик атомів компонентів для розрахунку можливого фазово-структурного стану сплавів та проведено порівняння із експериментальними даними. Дослідження мікроструктури показали наявність типової дендритної структури в литих сплавах з середнім розміром зерна на рівні 40 мкм, що залежить від концентрації складових елементів. Теоретично розраховану мікротвердість сплавів підтверджено експериментально. Виявилось, що розрахунок мікротвердості на основі концентрації валентних електронів, а також її залежності від об’ємного модуля та модуля зсуву дозволяє зрозуміти порядок величин мікротвердості.

СТРУКТУРА И МЕХАЧЕСКИЕ СВОЙСТВА ТУГОПЛАВКИХ МНОГОКОМПОНЕНТНЫХ СПЛАВОВ СИСТЕМИ Ta-Ti-V-Zr-Al

А. Левенец, М. Тихоновский, А. Великодный, Г. Ростова, И. Клименко, Г. Толстолуцкая

Были исследованы тугоплавкие высокоэнтропийные сплавы системы Ta-Ti-V-Zr-Al, в которой варьировалось содержание V и Ta. Предложены критерии на основе термодинамических параметров для бинарных сплавов, температур плавления компонентов, геометрических и электронных характеристик атомов компонентов для расчета возможного фазово-структурного состояния сплавов и сравнения с экспериментальными данными. Исследования микроструктуры показали наличие типичной дендритной структуры в литых сплавах со средним размером зерна на уровне 40 мкм, что зависит от концентрации составляющих элементов. Теоретически рассчитанная микротвердость сплавов была экспериментально подтверждена. Оказалось, что расчет микротвердости на основе концентрации валентных электронов, а также ее зависимости от объемного модуля и сдвига модуля позволяет понять порядок величин микротвердости.